



HAL
open science

A proximity-labeling proteomic approach to investigate invadopodia molecular landscape in breast cancer cells

Sylvie Thuault, Claire Mamelonet, Joëlle Salameh, Kevin Ostacolo, Brice Chanez, Danièle Salaün, Emilie Baudelet, Stéphane Audebert, Luc Camoin,
Ali Badache

► To cite this version:

Sylvie Thuault, Claire Mamelonet, Joëlle Salameh, Kevin Ostacolo, Brice Chanez, et al.. A proximity-labeling proteomic approach to investigate invadopodia molecular landscape in breast cancer cells. *Scientific Reports*, 2020, 10 (1), pp.6787. 10.1038/s41598-020-63926-4 . inserm-02859860

HAL Id: inserm-02859860

<https://inserm.hal.science/inserm-02859860>

Submitted on 8 Jun 2020

HAL is a multi-disciplinary open access archive for the deposit and dissemination of scientific research documents, whether they are published or not. The documents may come from teaching and research institutions in France or abroad, or from public or private research centers.

L'archive ouverte pluridisciplinaire **HAL**, est destinée au dépôt et à la diffusion de documents scientifiques de niveau recherche, publiés ou non, émanant des établissements d'enseignement et de recherche français ou étrangers, des laboratoires publics ou privés.



OPEN

A proximity-labeling proteomic approach to investigate invadopodia molecular landscape in breast cancer cells

Sylvie Thuault¹✉, Claire Mamelonet¹, Joëlle Salameh^{1,3}, Kevin Ostacolo^{1,4}, Brice Chanez^{1,5}, Danièle Salaün¹, Emilie Baudalet², Stéphane Audebert², Luc Camoin² & Ali Badache¹

Metastatic progression is the leading cause of mortality in breast cancer. Invasive tumor cells develop invadopodia to travel through basement membranes and the interstitial matrix. Substantial efforts have been made to characterize invadopodia molecular composition. However, their full molecular identity is still missing due to the difficulty in isolating them. To fill this gap, we developed a non-hypothesis driven proteomic approach based on the BioID proximity biotinylation technology, using the invadopodia-specific protein Tks5 α fused to the promiscuous biotin ligase BirA* as bait. In invasive breast cancer cells, Tks5 α fusion concentrated to invadopodia and selectively biotinylated invadopodia components, in contrast to a fusion which lacked the membrane-targeting PX domain (Tks5 β). Biotinylated proteins were isolated by affinity capture and identified by mass spectrometry. We identified known invadopodia components, revealing the pertinence of our strategy. Furthermore, we observed that Tks5 newly identified close neighbors belonged to a biologically relevant network centered on actin cytoskeleton organization. Analysis of Tks5 β interactome demonstrated that some partners bound Tks5 before its recruitment to invadopodia. Thus, the present strategy allowed us to identify novel Tks5 partners that were not identified by traditional approaches and could help get a more comprehensive picture of invadopodia molecular landscape.

While primary breast tumor patients can often be cured by surgery and/or radiation therapy combined to chemotherapy when detected at early stages, progression of the disease to the metastatic stage is still a major cause of patient death. Therefore, deciphering the molecular mechanisms underlying metastatic progression is of crucial importance for a better control of the disease. In order to reach the vascular system and be transported to distant organs and colonize them, tumor cells need to breach through basement membranes and invade through the interstitial matrix. Extracellular matrix (ECM) proteolysis is required to clear space and create tracks along which cells migrate. Invadopodia, which are dynamic actin-rich protrusive structures that cancer cells develop at their surface, play a major role in ECM proteolysis^{1–3}. Furthermore, increasing amount of evidence point to their involvement in metastasis^{4,5}. Therefore, a better understanding of their biology and molecular characteristics might permit the identification of markers of metastatic propensity and potential therapeutic targets.

Major efforts have been made during the past 25 years to characterize invadopodia molecular composition, using classical targeted proteomics involving cell fractionation or co-immunoprecipitation after cell lysis or candidate approaches. These studies have established that invadopodia are composed of structural and signaling proteins, including cortactin, cofilin, N-WASP and Tks4/5, that control the reorganization of the underlying actin cytoskeleton and the release of proteases such as MT1-MMP, involved in matrix degradation^{1–3}. Furthermore, time-lapse microscopy analyses revealed that invadopodia formation and maturation involve three major steps:

¹Centre de Recherche en Cancérologie de Marseille (CRCM), Aix-Marseille Univ, INSERM, Institut Paoli-Calmettes, CNRS, Marseille, France. ²CRCM, Marseille Proteomics, Aix-Marseille Univ, INSERM, CNRS, Institut Paoli-Calmettes, Marseille, France. ³Present address: INSERM UMR-S 1193, Univ. Paris-Sud, Université Paris-Saclay, Châtenay-Malabry, France. ⁴Present address: Department of Biochemistry and Molecular Biology, Biomedical Center, Faculty of Medicine, University of Iceland, Reykjavik, Iceland. ⁵Present address: Institut Paoli-Calmettes, Department of Medical Oncology, Marseille, France. ✉e-mail: sylvie.thuault@inserm.fr

initiation, assembly and maturation^{6,7}. However, the full molecular identity of these structures is missing due to the fact that their isolation and purification have been challenging⁸.

To circumvent these limits, we developed a non-hypothesis driven approach based on the proximity-dependent BioID biotinylation assay, coupled to mass spectrometry analysis⁹. This technique relies on the engineering of cells expressing a protein of interest fused to the promiscuous biotin ligase BirA*. In presence of biotin, BirA* biotinylates its close protein neighbors *in situ*, which can then be isolated using avidin-based affinity capture and identified by mass spectrometry. Proximity-dependent techniques allow to explore the molecular landscape of membrane-less organelles or of protein complexes localized to poorly soluble subcellular compartments, which are poorly accessible by more established approaches such as cell fractionation and affinity purification. Moreover, they enable the identification of weak or transient protein-protein interactions^{10,11}.

We wished to establish whether proximity labelling could help characterize invadopodia at the molecular level. For that purpose, the scaffold protein Tks5, also known as SH3PXD2A or FISH, was used as bait. Indeed, in contrast to other invadopodia components which are also components of other actin-based structures such as lamellipodia or focal adhesions, Tks5 is specific of invadopodia. Tks5 protein contains five Src Homology 3 (SH3) domains, proline-rich regions (PxxP) and, depending on the isoform, a N-terminal phox-homology (PX) domain which confers affinity for phosphatidylinositol-3,4-bisphosphate (PI(3,4)P₂)^{12,13}. Three Tks5 isoforms have been reported arising from distinct promoter usage: Tks5 α (also referred as Tks5long), Tks5 β and Tks5short^{14–16}. Tks5 α is the only isoform containing the N-terminal PX domain. In cancer, the expression level of Tks5 α or the ratio of Tks5 α expression to Tks5 β /Tks5short expression, rather than the total level of Tks5, is correlated to poor prognosis and lower metastasis-free survival in diverse cancer types^{15,17–20}. This is correlated with the fact that Tks5 α plays a major role in invadopodia formation and cancer cell invasion. Indeed, consequently to its recruitment at PI(3,4)P₂-enriched membrane domains, Tks5 potentiates actin polymerization through its interaction with the WASP-Arp2/3 complex²¹. Moreover, Tks5 α through direct or indirect recruitment of proteases at invadopodia contributes to ECM degradation^{22,23}. Finally, Tks5 facilitates the local generation of reactive oxygen species which are required for podosome (counterpart of invadopodia in normal cells) and invadopodia formation²⁴.

In this study, in order to determine Tks5 interactome *in situ* and therefore invadopodia molecular composition, we engineered MDA-MB-231 breast cancer cell lines expressing either Tks5 α , or Tks5 α lacking the PX domain fused to the biotin ligase BirA* and verified that this allowed the biotinylation and identification of invadopodia components. Label-free mass spectrometry analysis identified new potential invadopodia proteins that formed a protein-protein interaction network of actin cytoskeleton regulators. Tks5 α lacking the PX domain recruited an overlapping but distinct group of proteins indicating that some proteins associate to Tks5 before its recruitment to invadosomes. Thus, the present strategy shows great potential for the molecular characterization of invadopodia *in situ*.

Results

Selective biotinylation of invadopodia proteins by Tks5-BirA* fusion proteins. In order to characterize invadopodia at the molecular level, we set up the identification of the close neighbors of a specific component of invadopodia, the adaptor protein Tks5 α ¹², using the BioID proximity ligation technology. We therefore stably expressed wild type Tks5 α (Tks5) fused to BirA* in MDA-MB-231 breast cancer cells (Fig. 1A). We also generated MDA-MB-231 cells expressing a mutant form of Tks5 α lacking its PX domain (Δ PX-Tks5) fused to BirA* (Fig. 1A). This mutant, mimicking the Tks5 β /short form of Tks5, should not localize to invadopodia. Tks5 β has also been described to have a dominant negative effect over Tks5 α ¹⁵. Finally, cells expressing BirA* alone were established as control for identification of unspecific biotinylation. We derived individual clones by limiting dilution and selected cells with similar expression levels of the fusion proteins (Fig. 1C). Invasive cells form invadopodia when plated on an artificial ECM. Tks5-BirA* fusion proteins or BirA* expressing cells and non transfected (NT) cells were seeded on fluorescently-labeled gelatin to visualize invadopodia formation. We observed that Tks5-BirA* localized at mature invadopodia, identified by cortactin labeling and gelatin degradation, whereas Δ PX-Tks5-BirA* and BirA* did not (Fig. 1B). Moreover, in accordance with previous studies, Tks5-BirA* overexpression increased the ability of cells to degrade gelatin^{13,25}. Indeed, we observed an increase in the percentage of cells degrading the matrix, but also in the area that was degraded per individual cells (Fig. 1B,D,E), while expression of BirA* alone had no effect (data not shown). In contrast, expression of Δ PX-Tks5 reduced the percentage of degrading cells. These observations demonstrate that Tks5-BirA* fusion proteins are functional and that only full-length Tks5-BirA* is strongly enriched in invadopodia.

It was then important to verify that Tks5-BirA* could induce selective biotinylation at invadopodia. Cells were seeded on fluorescent gelatin in presence of biotin for 16 hours and localization of biotinylated proteins was assessed by staining with streptavidin coupled to Alexa Fluor 594. We observed an accumulation of biotinylated proteins at invadopodia in cells expressing Tks5-BirA*, but not in cells expressing the mutant Δ PX-Tks5-BirA* or BirA* alone (Fig. 2A and data not shown). In cells expressing Δ PX-Tks5-BirA*, biotinylated proteins were exclusively cytoplasmic. Thus this approach was likely to reveal invadopodia components.

Finally, we assessed if previously described partners of Tks5 and invadosomes components, such as N-WASP, Nck and Grb2^{21,25}, could indeed be biotinylated by Tks5-BirA*. MDA-MB-231 cells expressing Tks5-BirA* fusion proteins or BirA* were seeded on gelatin for 16 hours in the presence of biotin. Biotinylated proteins were isolated by affinity capture using avidin-coated beads and the biotinylation of the proteins of interest assessed by western blotting. N-WASP and Nck were biotinylated by Tks5-BirA* but not, or much less, by Δ PX-Tks5-BirA* (Fig. 2B). None of the proteins were biotinylated by BirA*. Thus our approach is capable of identifying *bona fide* Tks5 partners. This result also shows that the interactions of Tks5 with Nck and N-WASP, that have been previously identified by co-immunoprecipitation after cell lysis, also occurred *in vivo*. Furthermore, the fact that N-WASP and Nck were poorly biotinylated by Δ PX-Tks5-BirA* strongly suggested that their interaction with Tks5 occurred once Tks5 had been recruited at PI(3,4)P₂-enriched invadopodia. We cannot totally exclude,

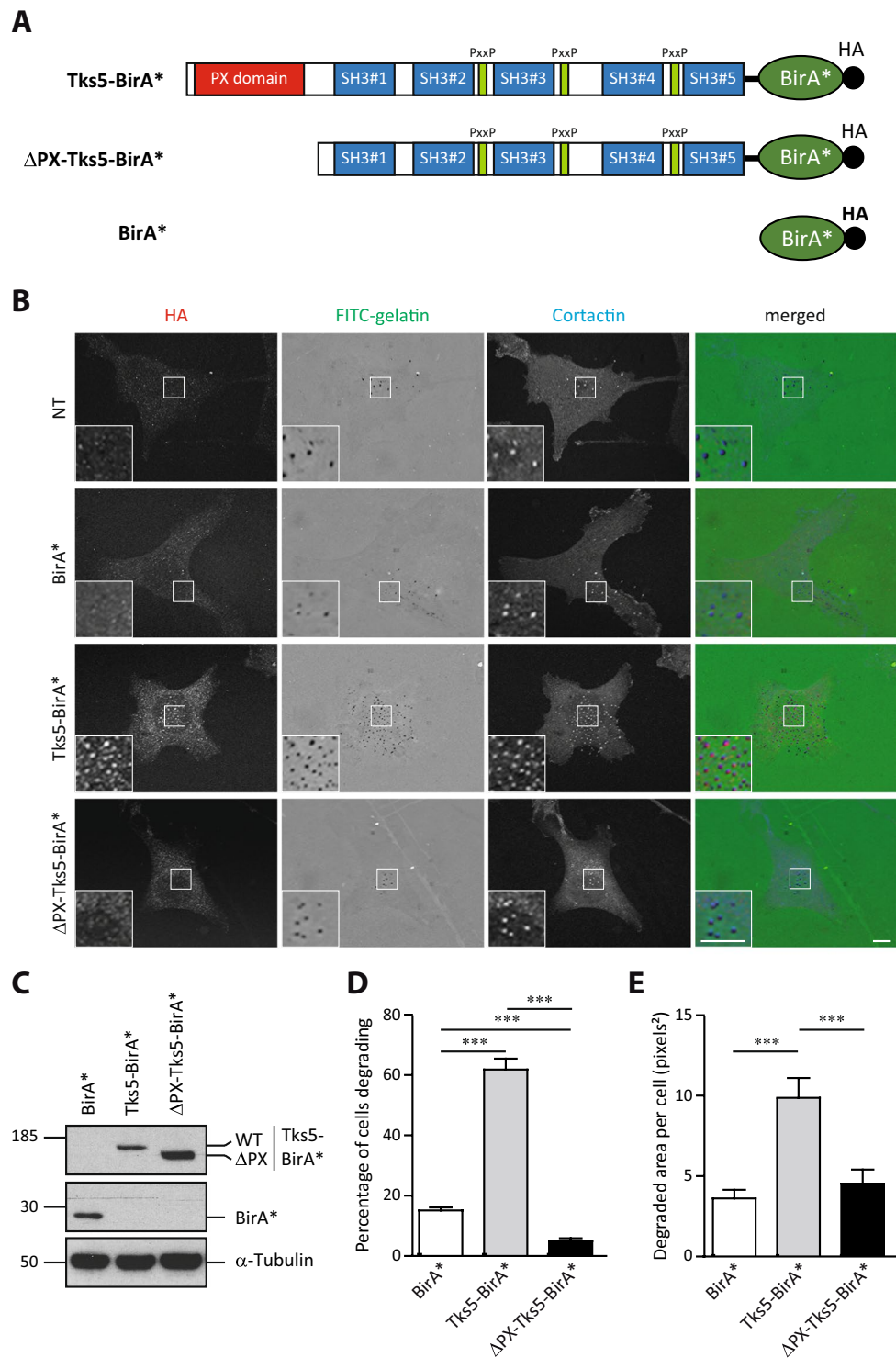


Figure 1. Tks5-BirA* is active and localizes in invadopodia. **(A)** Schematic representation of BirA* fusion proteins used in this study. The PX, SH3 and Proline rich (PxxP) domains of Tks5 are depicted. All fusion proteins have a HA tag at their C-terminus. **(B)** Representative images of MDA-MB-231 cells stably expressing wild-type Tks5 or Tks5 lacking its PX domain (Δ PX) fused to the biotin ligase BirA* or BirA* alone, and of non-transfected (NT) cells, seeded on fluorescently-labeled gelatin (FITC-gelatin) for 4 hours. Cells were fixed and stained with anti-HA and -cortactin antibodies. Invadopodia were identified thanks to cortactin labeling. Active invadopodia were identified thanks to degradation area (dark spots) in FITC-gelatin. The white-boxed regions are shown enlarged in the bottom insets. Scale bars represent 5 μ m. **(C)** Expression levels of BirA* fusion proteins in MDA-MB-231-derived cells described in **(B)** was assessed by western blotting using an anti-HA antibody. α -Tubulin was used as a loading control. **(D,E)** Tks5-BirA* fusion proteins are functional. The ability of MDA-MB-231 cells expressing Tks5-BirA* fusion proteins, described in **(B)**, to degrade

fluorescently-labeled gelatin was analyzed. The percentage of degrading cells (D) and the degraded area per cell (E) are represented as the mean \pm SEM of three independent experiments. *** $p \leq 0.001$. Full-length blots are presented in Supplementary Fig. 2.

however, that N-WASP and Nck require the presence of the PX domain for the interaction. By contrast, Grb2 was not biotinylated by Tks5-BirA* fusion proteins (Fig. 2B). This observation is in agreement with a previous study indicating that Grb2 can distinguish between invadopodia and podosomes²⁶. The lack of Grb2 biotinylation could also be due to improper relative orientation of the fused proteins and/or inaccessible lysine residues. Altogether these observations show that MDA-MB-231 cells expressing Tks5-BirA* and Δ PX-Tks5-BirA* are suitable cell models to address invadopodia composition in a global manner.

Tks5 α close neighbors belong to an integrative network associated with actin cytoskeleton reorganization.

Analysis of biotinylation in whole cell extracts or after affinity capture indicated that Tks5-BirA* fusion proteins led to high levels of biotinylation of a restricted number of proteins, whereas few proteins were biotinylated to detection levels in non-transfected MDA-MB-231 cells or cells expressing BirA* alone (Fig. 2C). Silver staining of the proteins pulled down in non-transfected cells or cells expressing BirA* revealed a substantial number of proteins binding non-specifically to avidin-coupled beads (Fig. 2D). We next conducted mass spectrometry analysis of affinity captured proteins from Tks5-BirA* expressing cells and control cells. Relative intensity-based label-free quantification (LFQ) method identified 40 proteins significantly enriched with a 1% permutation FDR (pFDR) in Tks5-BirA* pulldown compared to BirA* control pulldown (Fig. 3A and Supplementary Table S1).

To assess the biological relevance of this group of proteins, we surveyed the existence of previously described functional or physical protein-protein interactions (PPI) among them using the STRING platform. Such an analysis indicated that the identified Tks5 close neighbors form a significant functional network (PPI enrichment p-value = 1.54e-09). The significance of this network was even greater when WASL/N-WASP and NCK1/Nck, that we validated as close neighbors directly by western blotting (Fig. 2B), were included (PPI enrichment p-value = 1.17e-14). Application of Markov Clustering logarithm (MCL) revealed that Tks5 close neighbors are organized in a main core cluster (Fig. 3B - proteins in red and gold).

We next investigated molecular pathways associated with our biologically relevant network. Gene ontology analysis using PANTHER classification system indicated that “actin cytoskeleton organization” (GO: 0030036), critical for invadopodia regulation, was the most significantly overrepresented biological process in our network compared to its occurrence in the whole human genome (fold enrichment = 11.91, P value = 2.45e-10) strengthening the pertinence of our strategy (Fig. 3C,D).

Furthermore, comparison of Tks5 close neighbors identified in the present study to GLAD4U literature mining protein listing obtained for “invadosome” query and manual literature searching revealed that 17.5% (7 out of 40) were previously linked to invadosomes (Fig. 3A – red spots). Most of them have been implicated in invadosomes assembly through regulation of the actin cytoskeleton: Cortactin, a key component of invadopodia, which was among the most enriched biotinylated proteins with a fold enrichment (Log2) of 7.5 (Supplementary Table S1), is a regulator of Arp2/3 complex activity²⁷; and the Cdc42 guanine exchange factor FGD1^{28,29}, the formin binding protein FBP1 (FBP17)^{30–32}, the Ras-associated and pleckstrin homology containing protein 1 (RAPH1), also known as Lamellipodin (Lpd)³³, and the Drebrin-like protein, DBNL (mAbp1)³⁴ were all found to regulate invadosome formation through the control of factors implicated in elongation and branching of actin filaments. In contrast, the zonula occludens protein ZO-1/TJP1 was proposed to regulate degradative activity of invadopodia-like structures through its interaction with ADAM12 and MMP14^{35,36}. The ADAM15 metalloproteinase, which was actually suggested to be a Tks5 interactor^{22,37}, since its intracellular domain can associate with Tks5, might also function in degradation of the ECM, but, in contrast to ADAM12^{38,39}, its function in invadosomes remains to be demonstrated. Finally, the RNA binding protein IGF2BP2/IMP2 was shown to be involved in invadopodia formation through the control of the stability or localization of mRNAs of factors implicated in cell adhesion, mobility, invasion and ECM^{40,41}. We also identified factors that have not been themselves involved in invadosome biology, but belong to protein families whose other members have (Fig. 3A – orange spots). Such factors include the 5'-inositol lipid phosphatase Synaptojanin-1^{42,43}, the CIN85/CMS family member CD2AP/CMS⁴⁴ and the tight junction protein TJP2^{35,36}. Of note, the majority of these proteins constitute the main core cluster of the integrative network identified after MCL clustering (Fig. 3B). Additional proteins, including Reticulon-4 (RTN4)^{45,46}, PDZ and LIM domain protein 4 (PDLIM4/RIL)^{47,48} and Dihydropyrimidase-like protein 3 (DPYSL3/CRMP4)⁴⁹ were integrated to this main core cluster. Interestingly, these proteins, although not currently implicated in invadosome regulation, have been linked to actin cytoskeleton organization. Furthermore, as pointed out by the gene ontology analysis and manual literature searching, additional proteins involved in actin cytoskeleton organization were identified among Tks5 close neighbors (Fig. 3B – striped circles and Fig. 3D). These include the inhibitor of the Arp2/3 complex, Arpin⁵⁰, the breast cancer anti-estrogen resistance protein 3 (BCAR3)^{51,52}, the PDZ and LIM domain protein 1 (PDLIM1/ELFIN)^{53,54}, the SHC-transforming protein 1 (SHC1)⁵⁵, the LIM and Calponin homology domain containing protein 1 (LIMCH1)⁵⁶, the E3 ubiquitin ligase Mind Bomb 1 (MIB1)⁵⁷, the microtubule-associated protein 4 (MAP4)⁵⁸ and the anthrax toxin and collagen I receptor, ANTXR1/TEM8^{59,60}. These observations strongly suggest that, through their control of actin organization, these proteins could be involved in invadosome formation.

Thus, although other biological processes such as “D-ribose metabolism” or “tRNA wobble base modification”, were found significantly overrepresented by PANTHER classification system, the main pathway represented among Tks5 interactome is linked to actin cytoskeleton organization, which is critical for invadopodia regulation

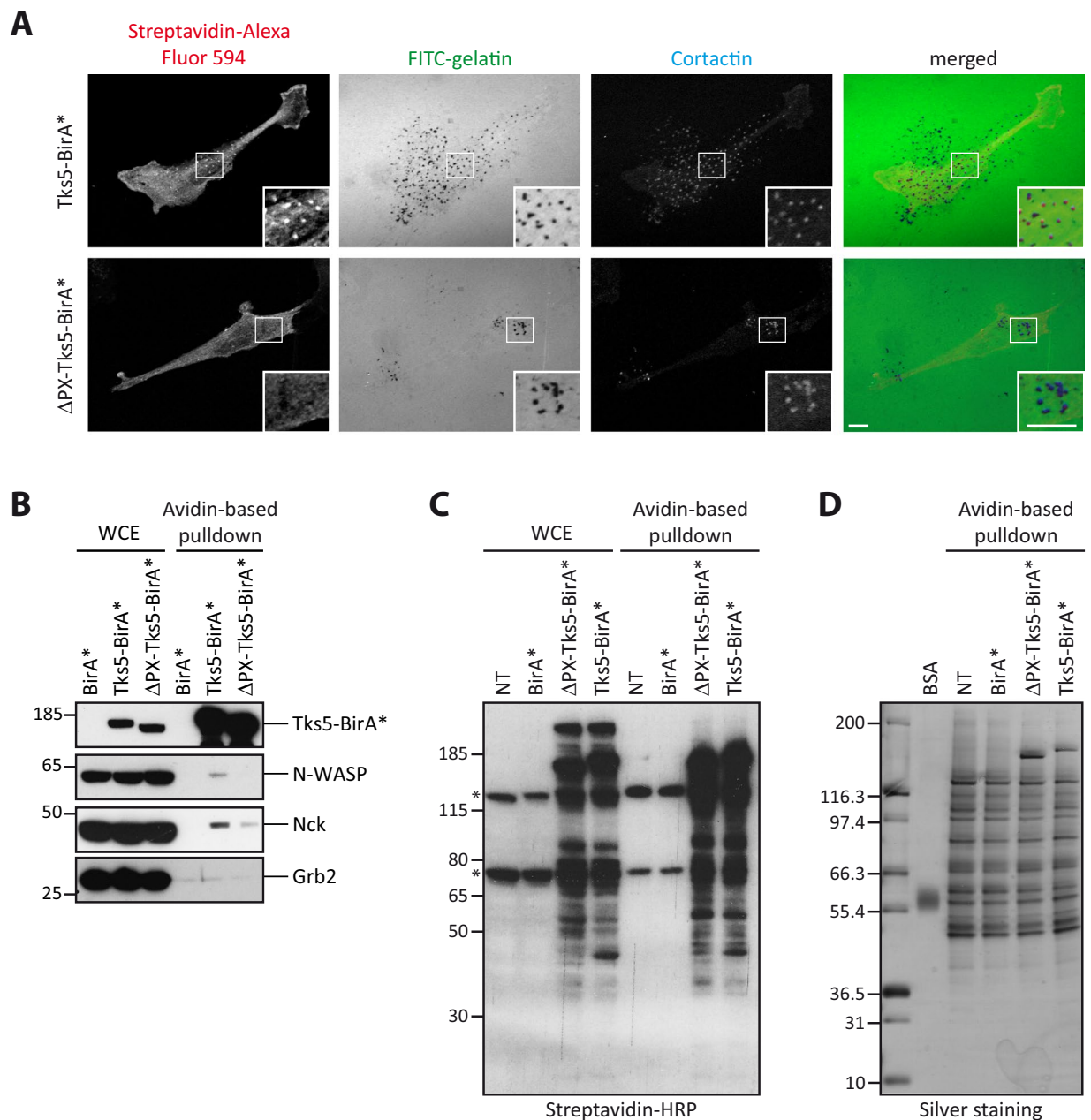


Figure 2. Selective biotinylation of invadopodia proteins by Tks5-BirA*. **(A)** Representative images of MDA-MB-231 cells stably expressing Tks5-BirA* or ΔPX-Tks5-BirA* seeded on fluorescently-labeled gelatin (FITC-gelatin) in the presence of biotin for 16 hours. Cells were fixed and stained for cortactin as a marker of invadopodia and streptavidin coupled to Alexa Fluor 594 to reveal biotinylated proteins. The white-boxed regions are shown enlarged in the bottom insets. Scale bars represent 5 μm. **(B)** Analysis of the biotinylation of known Tks5 interactors and of well characterized invadosome components. MDA-MB-231 cells stably expressing BirA*, Tks5-BirA* or ΔPX-Tks5-BirA* were seeded on gelatin in presence of biotin for 16 h. After cell lysis, biotinylated proteins were isolated by affinity capture using avidin-coated beads. The presence of proteins of interest was assessed in whole cell extract (WCE) or after avidin-based pull-down by western blotting with specific antibodies. **(C)** Isolation of proteins biotinylated by Tks5-BirA* and ΔPX-Tks5-BirA*. MDA-MB-231 cells stably expressing Tks5-BirA*, ΔPX-Tks5-BirA* or BirA*, and non-transfected (NT) cells were seeded on gelatin and treated with biotin for 16 h before cell lysis. Biotinylated proteins were pulled down via avidin-coated beads. The presence of biotinylated proteins was assessed by western blotting in whole cell extract (WCE) or after avidin-based pull-down (one-twentieth of the total pull-down was used) using HRP-coupled streptavidin. (*) corresponds to intrinsically biotinylated proteins. **(D)** One-tenth of the samples shown in (C) was resolved by SDS-PAGE for silver staining of the isolated proteins; the rest was analyzed by mass spectrometry. Full-length blots/gels are presented in Supplementary Fig. 2.

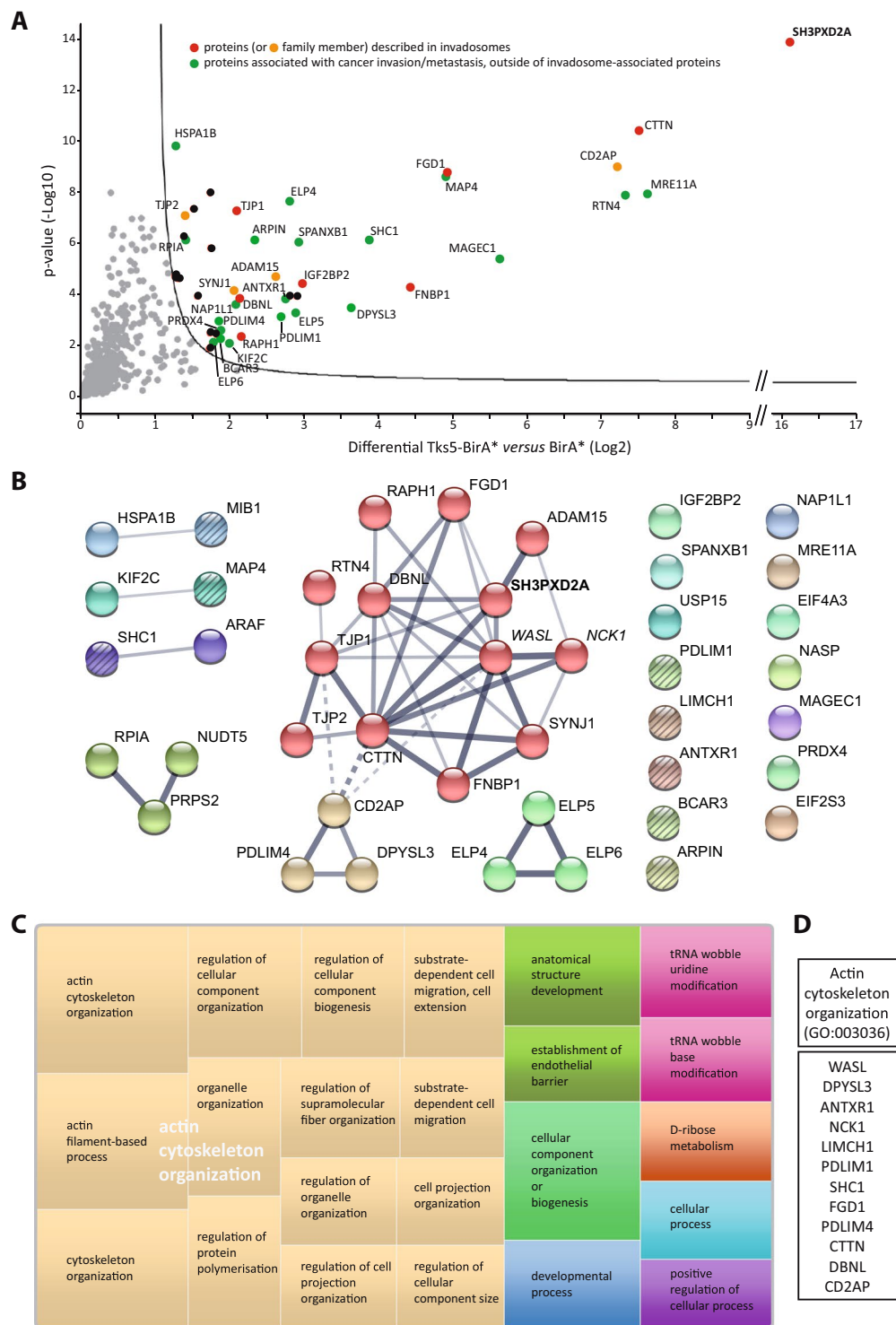


Figure 3. Tks5 α close neighbors belong to an integrative network related to actin cytoskeleton reorganization. MDA-MB-231 cells expressing Tks5-BirA* or BirA* were seeded on gelatin-coated plates and treated with biotin for 16 h. Biotinylated proteins were isolated by affinity capture and identified by mass spectrometry. **(A)** Volcano plot showing the differential level (Log2) and the p-value (-Log10), on x and y axis, respectively, for Tks5-BirA* versus BirA*. The full line is indicative of protein hits obtained at a permutation false discovery rate (pFDR) of 1%. Data result from two different experiments processed three times. Red and orange spots highlight proteins previously associated with invadosomes and proteins for which a family member has been associated with invadosomes, respectively. Green spots highlight proteins associated with cancer invasion/metastasis, outside of invadosome-associated proteins. For more details, refer to Supplementary Table S1. **(B)** Proteins biotinylated by Tks5-BirA*, including the validated candidate proteins (WASL and NCK1 which appear in italic) were integrated in a protein-protein interaction network based on physical and functional interactions per the STRING database. Markov Clustering algorithm has been applied. Proteins belonging

to a same cluster have an identical color; the main core cluster is in red and gold. Line thickness indicates the strength/confidence of data support. Dotted lines mark the edges of the clusters. Among disconnected proteins, factors linked to actin organization are striped. The bait Tks5/SH3PXD2A is highlighted in bold. (C) Treemap representing the top biological processes represented among proteins biotinylated by Tks5-BirA*, as defined in (B), using PANTHER classification system for analysis and REVIGO for summarization and visualization. Each rectangle is a single cluster representative. The representatives are joined into ‘superclusters’ of loosely related terms, visualized with different colors. Size of the rectangles reflects the *p*-value of the GO term. (D) Proteins biotinylated by Tks5-BirA* (B) categorized as GO “Actin cytoskeleton organization” by PANTHER classification system.

(Fig. 3C). Furthermore, a large fraction (more than 50%) of Tks5 close neighbors identified here (Fig. 3A and Supplementary Table S1) is associated with cancer cell invasion and metastasis.

Invadopodia components show different modes of interaction with Tks5. To obtain further insights in the comprehension of invadopodia formation, we took advantage of the cellular model expressing the short form of Tks5, deleted of its PX domain (Δ PX-Tks5) (Fig. 1). PX domains mediate interactions with specific membrane phosphoinositides. Tks5 PX domain was reported to preferentially interact with PI(3)P and PI(3,4)P₂²². Such interaction contributes to Tks5 activation and thus to podosomes and invadopodia formation^{13,21,61}. Our cellular model could therefore help us differentiate factors that associate with Tks5 before its recruitment to invadosome precursors, from those that associate with Tks5 at invadosome precursors. We therefore analyzed mass spectrometry data resulting from Δ PX-Tks5-BirA* pulldowns and identified 44 enriched proteins at 1% pFDR in Δ PX-Tks5-BirA* pulldown relatively to BirA* control pulldown (Supplementary Table S2). We then intersected this list of proteins with the *in situ* Tks5 interactome (Fig. 4A and Supplementary Table S3). Twenty-seven proteins were shared (Fig. 4A - red spots and Supplementary Table S3), corresponding to more than half of the total proteins identified in each condition (67.5% and 61.3% of Tks5-BirA*- and Δ PX-Tks5-BirA*-associated proteins respectively). Some proteins were similarly enriched in the Tks5-BirA*- and Δ PX-Tks5-BirA*-associated groups, including the key invadopodia component Cortactin. Western blotting after pulldown of biotinylated proteins confirmed that Cortactin was biotinylated at similar levels by Tks5-BirA* and Δ PX-Tks5-BirA*, indicating that Cortactin is in the vicinity of Tks5 independently of its presence at invadopodia (Fig. 4B). Many proteins were found exclusively or more strongly associated with Tks5-BirA* than Δ PX-Tks5-BirA*, among which thirteen were specifically biotinylated by Tks5-BirA*, but not by Δ PX-Tks5-BirA* nor BirA* (Fig. 4A - blue spots and Supplementary Table S3). RTN4, FGD1 and SHC1 were among the most highly enriched (Difference (Log2)>3.35). We confirmed by western blotting after pulldown of biotinylated proteins that RTN4 and FGD1 were specifically biotinylated by Tks5-BirA* (Fig. 4B) and that SHC1, MAP4 and CD2AP/CMS were biotinylated by both fusion proteins, but were more tightly associated with Tks5-BirA* (Fig. 4B). We can speculate that the interaction of SHC1, MAP4 and CD2AP is stabilized once Tks5 is recruited to PI(3,4)P₂-enriched domains. Finally, for some of the shared proteins, fold enrichment was higher with Δ PX-Tks5-BirA* than with Tks5-BirA*, in accordance with the proposed mechanism whereby Δ PX-Tks5 might inhibit invadosome formation by mislocalizing actin-regulatory proteins⁶². One might be concerned that expression of endogenous Tks5 might compete with Tks5-BirA* fusion proteins, disturbing full interaction with their partners; however we have verified that biotinylation of all validated partners is unchanged upon endogenous Tks5 knockdown (Sup.Fig. 1). Overall the comparison of Tks5 α and Tks5 β (Δ PX-Tks5) interactomes identifies three groups of Tks5 partners: (1) those interacting with Tks5 before its recruitment to PI(3,4)P₂-rich domain, (2) those interacting weakly with Tks5 before its recruitment to PI(3,4)P₂-rich domain, but whose interaction is stabilized once Tks5 is recruited, and (3) those interacting with Tks5 at invadopodia.

Finally, we wished to verify if newly identified Tks5 partners, for which we identified antibodies suitable for immunofluorescence staining, localized to invadopodia. As invadopodia labelling for proteins that are also highly expressed in the cytoplasm, such as the endoplasmic reticulum-associated RTN4/Nogo-B or the cytosolic scaffold SHC1, was challenging, we adapted a protocol for immunostaining after removal of the cell body by hypotonic shock and hydrodynamic force⁶³, preserving only the invadopodia within the gelatin matrix. We observed that RTN4/Nogo-B and SHC1 could localize at mature invadopodia, after removal of the cell body, but also in intact cells (Fig. 5). In contrast, MAP4 does not seem to localize at invadopodia (data not shown). However, RTN4/Nogo-B and SHC1 were found less often at degradation foci than cortactin or the metalloprotease MT1-MMP, indicating that their presence at invadopodia might be transient. This suggests that these proteins, rather than being constitutive invadopodia components, might have a stage-specific regulatory function.

Discussion

Invadopodia, actin-rich protrusive structures developed at cancer cells surface in order to degrade the surrounding ECM¹⁻³, are correlated to the metastatic potential of diverse cancer types, hence the importance of better understanding their biology^{4,5}. In the current study, in order to gain insights into invadopodia molecular landscape, we determined the *in situ* interactome of Tks5, a key player in invadosome formation, by a global approach based on proximity-dependent labeling. Previous studies have identified Tks5 interacting partners^{21,22,25,59} using conventional approaches, based on identification of proteins co-precipitating with Tks5 or Tks5 domains, e.g. the SH3 domains. Proximity-dependent labeling methods in living cells are powerful technologies that allow to explore protein-protein interactions (PPI), or at least protein-protein close proximity, *in situ*, before cell lysis. Unlike more classical approaches, it allows to identify PPI in more physiologically relevant conditions, low affinity and/or transient PPI, as well as the proteome of membrane-less organelles and subcellular domains^{10,11}. We

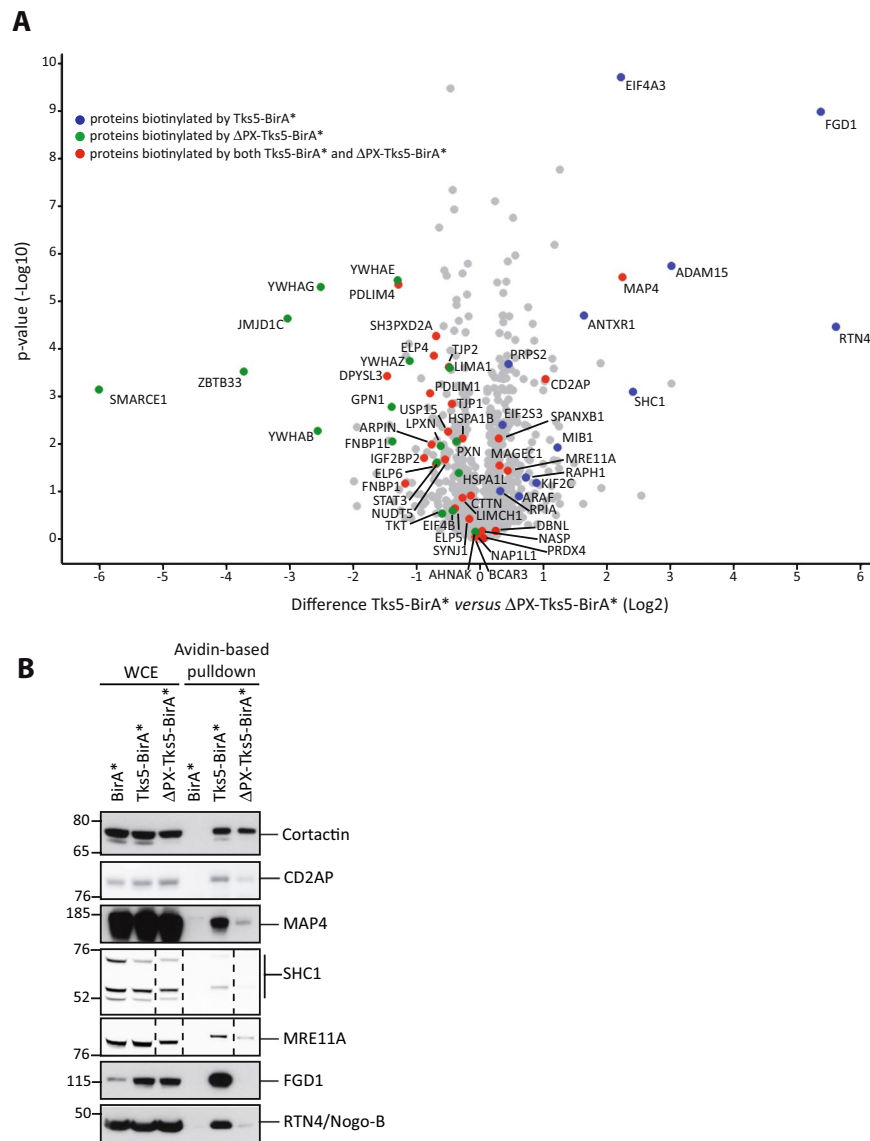


Figure 4. Invadopodia components show different modes of interaction with Tks5. MDA-MB-231 cells expressing Tks5-BirA*, ΔPX-Tks5-BirA* or BirA* were seeded on gelatin-coated plates and treated with biotin for 16 h. Biotinylated proteins were isolated by affinity capture and identified by mass spectrometry. **(A)** Volcano plot showing the differential level (Log2) and the p-value (-Log10), on x and y axis, respectively, for Tks5-BirA* versus ΔPX-Tks5-BirA*, without taking into account proteins identified as biotinylated in BirA* control condition. Data result from two different experiments processed three times. Proteins biotinylated by Tks5-BirA*, by ΔPX-Tks5-BirA* and by both Tks5-BirA* and ΔPX-Tks5-BirA*, relative to the BirA* control condition, are highlighted in blue, green and red, respectively. For more details refer to Supplementary Table S3. **(B)** Verification of the biotinylation levels induced by Tks5-BirA* or ΔPX-Tks5-BirA*, of selected proteins identified in (A). The presence of proteins of interest was assessed in whole cell extract (WCE) or after avidin-based pulldown followed by western blotting with the indicated antibodies. Dotted lines indicate that the disposition of the lanes has been reorganized, but that lanes are from a single blot and are therefore directly comparable. Full-length blots are presented in Supplementary Fig. 2.

choose to fuse Tks5 to the promiscuous biotin ligase BirA*. Fusion of BirA* to Tks5 did not affect its function: it was strongly enriched in invadopodia and promoted invadopodia formation and activity (Fig. 1). Biotinylation is supposed to occur within an estimated range of 10nm⁶⁴. Thus Tks5-BirA* should mostly biotinylate direct partners of Tks5, and proteins that belong to invadopodia, which have an estimated diameter of 0.05 to 1μm. We verified that Nck and N-WASP, invadopodia proteins and co-precipitation partners of Tks5, are indeed biotinylated by Tks5-BirA*, but only when present at invadopodia (Fig. 2). This result also confirms that these interactions actually take place in intact cells.

Mass spectrometry analysis identified at least 40 proteins significantly associating with Tks5 (Fig. 3 and Supplementary Table S1). A large number of the identified proteins are part of a functionally and physically-linked integrative network. Around twenty percent of Tks5 proximate proteins, or their homologs, have been previously

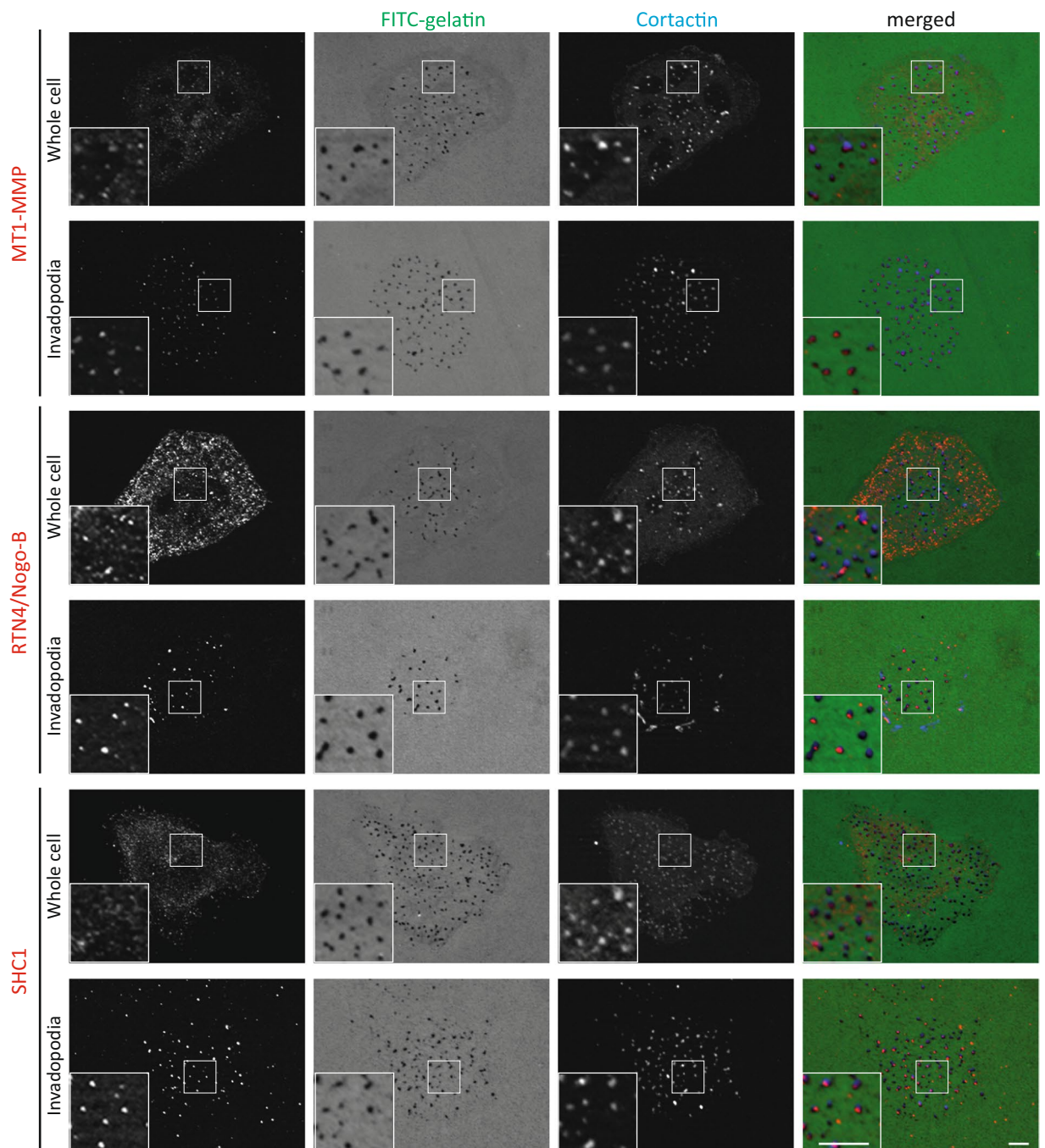


Figure 5. RTN4/Nogo-B and SHC1, newly identified Tks5 close neighbors, localize at a subset of mature invadopodia. Representative images of MDA-MB-231 cells stably expressing Tks5-BirA* seeded on fluorescently-labeled gelatin (FITC-gelatin) for 4 hours. In the “Whole cell” condition, cells were kept intact, whereas in the “Invadopodia” condition, cell bodies were removed by hypotonic shock and hydrodynamic force, before fixation. Cells were stained with the indicated antibodies. Cortactin being a constitutive component of invadopodia, cortactin staining (in blue) was used as a control. Scale bars represent 2.5 μm .

linked to invadosomes and more than 50% are involved in cancer invasion and metastasis, revealing Tks5 *in situ* interactome as a source of potential new invadopodia components and regulators and strengthening the relevance of our approach. Very few studies have addressed the proteome of invadosomes, as their isolation and purification have been challenging. Two strategies have been used before: either cell fractionation by mechanical removal of the cell bodies in the case of invadopodia and podosomes^{65,66} or laser microdissection in the case of Src-induced rosettes⁵⁷. Although our list of proteins shares only few proteins with these studies (none with Attanasio *et al.*, 1 with Cervero *et al.*, 5 with Ezzoukhry *et al.*), a common feature between these studies and our results is the overrepresentation of factors involved in actin cytoskeleton organization (Fig. 3). We could also identify proteins linked to metabolism and transcription/protein synthesis. However, in contrast to these studies in which these

categories of proteins were highly enriched, they were poorly represented in our study. These differences might be linked to the strategy used. Whereas classical proteomic approaches caught a snapshot of invadosomes protein composition, proximity biotinylation captured Tks5 neighbors over an extended period (16 h), which should also reveal transiently associated proteins. Actually, partial co-localization of RTN4/Nogo-B and SHC1 with mature invadopodia suggests that they might only transiently associate with Tks5, at a specific step of invadopodia lifetime (Fig. 5). Moreover, whereas previous studies were based on cellular fractionation of the whole invadosomes, our strategy is focused on the identification of partners of a particular invadopodia protein. Considering the volume of an invadopodia, invadopodia components are not necessarily in the vicinity of Tks5, and one does not expect a complete overlap between Tks5 interactome and the invadopodia proteome. Tks5 being usually depicted as localizing in the functional core of invadosomes in close proximity of factors regulating actin polymerization and ECM degradation, it is not surprising to predominantly identify factors linked to these processes among Tks5 close neighbors. Even though the biotinylation radius of BirA* is low, we cannot exclude that some of the proteins identified in Tks5 neighborhood, might be indirect partners. However, assessing molecular organization of Tks5 close neighbors using InterPro database, we observed that 17 out of 40, including the known invadopodia components FGD1, RAPH1 and FNBP1, contain either Pro-rich regions or SH3 domains, that could mediate a direct interaction with Tks5 (Supplementary Table S1). Further studies will be necessary to address their specific mode of interaction.

Assembly of invadopodia is a sequential process starting with the formation of an invadopodium precursor that will be stabilized and finally mature into a degradation-competent invadopodium^{1,67}. Tks5 plays a major role in the stabilization step through interaction of its PX domain to PI(3,4)P₂-enriched domains, and as a scaffolding protein allowing the recruitment of factors necessary for invadopodium maturation⁶¹. Our comparison of the *in situ* interactomes of Tks5 α (Tks5) and of its short form Tks5 β (Δ PX-Tks5) suggests that, additionally to acting as a scaffolding factor in invadopodia-to-be PI(3,4)P₂-rich domains, Tks5 associates with key invadopodia regulators, e.g. Cortactin, independently of its recruitment to invadopodia. Although these results allow us to get a first insight into the molecular mechanism of recruitment of proteins found in the vicinity of Tks5, further work would be necessary to address the spatiotemporal organization of invadopodia.

Overall, the present study demonstrates that proximity-dependent labeling methods in living cells are suitable to get an insight of invadopodia molecular composition. Indeed, we identified known invadopodia components/regulators and new potential invadopodia players for which validation of their implication in invadopodia activity and eventually in metastases formation, is needed. However, the fact that we did not identify Nck and N-WASP in the global strategy, while we identified them as Tks5 close neighbors by a targeted strategy, points to limits in sensitivity of our strategy and suggest possible routes of improvements. Several options are under investigation to increase the sensitivity of mass spectrometry detection, including the use of a more efficient promiscuous biotin ligase (e.g. TurboID) or the enhancement of the biotinylation range through the expansion of the linker region between the enzyme and the bait^{68,69}. These strategies combined to the identification of the *in situ* protein neighbors of additional specific invadopodia components, such as Tks4, would permit to get a larger coverage of the invadopodia proteome. We can also envision to use such proximity-dependent labeling approaches to study the molecular composition of podosomes developed by normal cells and of the various types of invadopodia cancer cells differentially assemble during the invasion process, depending on the matrix environment^{70,71}. The slow kinetics of BirA* precludes its use for studying the dynamic molecular organization of invadopodia which have a lifetime in the order of one hour. Dynamics could be addressed by next generation proximity-dependent labeling techniques, such as the modified peroxidase APEX2 or TurboID, that might allow to resolve spatiotemporal regulation of invadopodia at the minute-scale^{68,72}. The very existence of invadopodia or invadopodia-like structure in a physiological context, i.e. during tumor cell invasion, has been debated for years. As proximity-dependent approaches can also be applied *in vivo*^{73–75}, our study opens the door to the development of proximity-dependent labeling approaches in *in vivo* models of invasion more relevant to metastatic progression.

Materials and Methods

Cell lines. MDA-MB-231 cells were cultured in Dulbecco's Modified Eagle Medium (Thermo Fisher), supplemented with 10% fetal bovine serum (Eurobio, Courtaboeuf, France) at 37 °C in a humidified atmosphere with 5% CO₂, and checked regularly for mycoplasma contamination. Stable MDA-MB-231 cell lines were generated by transfection of the BirA* plasmid constructs by Lipofectamine 2000 (Invitrogen) and selection with 1 mg/ml geneticin. Individual clones were generated by limiting dilution. Ten to twenty clones were screened for BirA* fusion proteins expression levels. The degradative activity of three to four clones with different expression levels for each BirA* fusion protein was assessed to verify that Tks5 fusion proteins actually promoted (Tks5-BirA*) or inhibited (Δ PX-Tks5-BirA*) cell degradative activity. Clones expressing similar levels of the transgenes were selected for further analysis.

Plasmid constructs. Wild type Tks5 and the mutant Tks5 lacking its PX domain, without stop codon, were amplified by PCR from pGFP-N1-Tks5 (a kind gift from S. Courtneidge) with appropriate primers (Supplementary Table S4), used to generate pDONR-Tks5 and pDONR- Δ PX-Tks5, respectively before their sub-cloning in the destination vector pcDNA3.1 MCS-BirA(R118G)-HA (modified from Addgene plasmid # 36047, a kind gift from K. J. Roux) by Gateway technology to obtain Tks5 and Δ PX-Tks5 fused to the N-terminus of BirA*-HA. All constructs were sequence verified.

Antibodies. Rabbit antibodies against Tks5 (M-300), MAP4 (H-300), HA (Y-11) and mouse antibody against Grb2 (C-7) were purchased from Santa Cruz Biotechnology. Mouse antibody against Cortactin (clone 4F11) was purchased from Millipore. Antibodies against N-WASP (mouse, ab56454), NogoA/B (rabbit, ab47085), CD2AP

(rabbit, ab205017), MMP14/MT1-MMP (rabbit, ab51074) and MRE11 (mouse, ab214) were from Abcam. Rabbit antibody against SHC1 (610081) and mouse antibodies against Nck (610099) and SHC1 (610879) were from BD Transduction Laboratories. Anti- α -Tubulin (mouse, clone DM1A) and anti-FGDI (rabbit, HPA000911) were from Sigma Life Science. Biotinylated proteins were detected either by Alexa Fluor594 Streptavidin (405240, BioLegend) or Streptavidin-HRP (21130, Thermo Scientific).

Proximity biotinylation. Cells stably expressing BirA* fusion proteins were seeded on gelatin-coated plates and treated overnight with 50 μ M biotin, then lysed in a buffer composed of 50 mM Tris pH 7.4, 500 mM NaCl, 0.4% SDS, 2% Triton X-100, 5 mM EDTA and 1 mM DTT supplemented with protease and phosphatase inhibitors. Biotinylated proteins were isolated by incubating the cell lysates with Avidin-coated beads (Thermo Fisher) for 1 h at 4 °C. After three washes with lysis buffer and one wash with 50 mM Tris pH 7.4 plus 50 mM NaCl, beads were resuspended in SDS loading buffer supplemented with 2 mM D-biotin (Invitrogen).

Western blotting. After protein extracts preparation, quantification and denaturation in SDS loading buffer, samples were run on Novex NuPAGE Bis-Tris 4–12% gels using a MOPS based running buffer. Proteins were transferred onto nitrocellulose membranes, incubated with primary antibodies and secondary antibodies coupled to HRP and detected by chemoluminescence.

Mass spectrometry analysis. Biological samples were prepared in duplicate and each sample was further analyzed thrice by liquid chromatography (LC)-tandem mass spectrometry (MS/MS). Protein extracts were stacked on NuPAGE 4–12% Bis-Tris acrylamide gels (Life Technologies) and cut from the gel. Gels pieces were submitted to an in-gel trypsin digestion⁷⁶. Pooled extracts were dried down in a centrifugal vacuum system and samples were reconstituted and analyzed by LC-MS/MS using an LTQ Velos Orbitrap Mass Spectrometer (Thermo Electron, Bremen, Germany) online with an Ultimate 3000RSLCnano chromatography system (Thermo Fisher Scientific, Sunnyvale, CA). Peptides were separated on a Dionex Acclaim PepMap RSLC C18 column (15 cm \times 75 μ m I.D, 100 Å pore size, 2 μ m particle size) at 300 nL/min flow rate. Peptides were eluted by a two steps linear gradient (4–22% acetonitrile/H₂O; 0.1% formic acid for 110 min and 22–32% acetonitrile/H₂O; 0.1% formic acid for 10 min). For peptide ionization in the EASY-Spray nanosource, spray voltage was set at 1.9 kV at 275 °C. MS spectra were acquired in the Orbitrap in the range of m/z 300–1700 at a FWHM resolution of 30 000 and using the 445.120025 ions as internal mass calibration. Collision-induced dissociation fragmentation was performed in the ion trap on the 10 most intense precursor ions. The signal threshold for an MS/MS event was set to 500 counts. Dynamic exclusion was enabled with a repeat count of 1, exclusion list size 500 and exclusion duration of 30 s.

Protein identification and quantification. Relative intensity-based label-free quantification (LFQ) was processed using MaxQuant, version 1.6.3.4^{77,78} using mainly default parameters. The acquired raw LC-MS/MS data were first processed using the integrated Andromeda search engine⁷⁹. Spectra were searched against the Human database (UniProt Proteome reference, date 2019.01; 20412 entries) supplemented with a set of 245 frequently observed contaminants. The match between runs option was enabled to transfer identifications across different LC-MS/MS replicates based on their masses and retention time using default parameters. The quantification was performed using a minimum ratio count of 1 (unique+razor) and the second peptide option to allow identification of two co-fragmented co-eluting peptides with similar masses. For identification, the false discovery rate (FDR) at the peptide and protein levels were set to 1%. The statistical analysis was done with Perseus program (version 1.6.1.3) (<http://www.maxquant.org>) using LFQ normalised intensities. First, proteins marked as contaminant, reverse hits, and “only identified by site” were discarded. Protein LFQ normalized intensities were base 2 logarithmized to obtain a normal distribution. Quantifiable proteins were defined as those detected in at least 70% of the samples in one or more condition. Missing values were replaced using data imputation using default parameters. Differential proteins were selected using a two-sample t-test using permutation based FDR-controlled at 0.01 and employing 250 permutations. The p value was adjusted using a scaling factor s_0 with a value of 1⁸⁰. The mass spectrometry proteomics data, including search results, has been deposited to the ProteomeXchange Consortium (www.proteomexchange.org)⁸¹ via the PRIDE⁸² partner repository with the dataset identifier PXD015847.

Proteome analysis. Gene ontology (GO) and enrichment analyses were performed using the Protein Analysis Through Evolutionary Relationships (PANTHER 14.1) (<http://pantherdb.org/>)^{83,84} using the whole human genome as background. REVIGO web server was used to summarize and visualize GO terms (<http://revigo.irb.hr/>)⁸⁵. Interaction network were generated using STRING's website (version 11.0) at high confidence (0.7) and network was clustered using a Markov Clustering algorithm “MCL inflation parameter = 3” (<https://string-db.org/>)^{86,87}.

Matrix degradation assay, cell fractionation and immunofluorescence. Acid-treated coverslips were incubated with 50 μ g/ml poly-D-lysine 20 min at 37 °C, then with 0.5% glutaraldehyde 15 min at room temperature (RT) and then inverted on a 40 μ l drop of 0.2% gelatin plus Oregon Green 488–conjugated gelatin (Life Technologies) (10:1) mixture 10 min at RT. The gelatin matrix was then quenched with 5 mg/ml sodium borohydride 5 min at RT and dehydrated in 70% EtOH for storage. Thirty thousand MDA-MB-231 cells were plated for 4 h on gelatin-coated coverslips rehydrated in complete growth medium for 1 h before use. For removal of the cell bodies, cells were incubated within 2.5 mM Triethanolamine hypotonic buffer for 3 min, then cell bodies were removed with hydrodynamic force by the pipetting “up and down” of cold PBS plus inhibitors of proteases and phosphatases for 20–25 times, before a final wash with the same solution and fixation. This protocol

is adapted from Kuo *et al.*⁶³. Cells were then fixed with 4% formaldehyde in PBS, permeabilized with 0.1% Triton X-100 and blocked with 1% BSA. Immunolabeling was performed with antibodies directed against target proteins and secondary antibodies labeled with DyLight 405 or AlexaFluor 594 (Jackson ImmunoResearch). Images were acquired on a Zeiss structured light ApoTome microscope equipped with a 63×1.4 Plan-Apochromat objective. Percentage of cells degrading was assessed by imaging 10 random fields per condition. Matrix degradation was analyzed by quantifying the mean degraded area in pixels per cell using a home-made Fiji macro. Twenty-five cells per condition per experiment were analyzed to quantify matrix degradation.

Statistical analysis. All statistical analyses were performed using GraphPad Prism software. The unpaired one-tailed *t* test, with Welch correction, and the Mann Whitney test, were used to determine significant differences between data groups. Graphs were plotted using Prism, to show the mean and SEM. P values are indicated on the graph as *P < 0.05, **P < 0.01, ***P < 0.001.

Received: 2 December 2019; Accepted: 6 April 2020;

Published online: 22 April 2020

References

- Eddy, R. J., Weidmann, M. D., Sharma, V. P. & Condeelis, J. S. Tumor Cell Invadopodia: Invasive Protrusions that Orchestrate Metastasis. *Trends Cell Biol.* **27**, 595–607 (2017).
- Linder, S., Wiesner, C. & Himmel, M. Degrading devices: invadosomes in proteolytic cell invasion. *Annu. Rev. Cell Dev. Biol.* **27**, 185–211 (2011).
- Weaver, A. M. Invadopodia: Specialized Cell Structures for Cancer Invasion. *Clin. Exp. Metastasis* **23**, 97–105 (2006).
- Meirson, T. & Gil-Henn, H. Targeting invadopodia for blocking breast cancer metastasis. *Drug Resist. Updat.* **39**, 1–17 (2018).
- Paterson, E. K. & Courtneidge, S. A. Invadosomes are coming: new insights into function and disease relevance. *FEBS J.* **285**, 8–27 (2018).
- Beatty, B. T. & Condeelis, J. Digging a little deeper: The stages of invadopodium formation and maturation. *Eur. J. Cell Biol.* **93**, 438–444 (2014).
- Murphy, D. A. & Courtneidge, S. A. The ‘ins’ and ‘outs’ of podosomes and invadopodia: characteristics, formation and function. *Nat. Rev. Mol. Cell Biol.* **12**, 413–426 (2011).
- Havrylov, S. & Park, M. MS/MS-based strategies for proteomic profiling of invasive cell structures. *Proteomics* **15**, 272–286 (2015).
- Roux, K. J., Kim, D. I., Raida, M. & Burke, B. A promiscuous biotin ligase fusion protein identifies proximal and interacting proteins in mammalian cells. *J. Cell Biol.* **196**, 801–810 (2012).
- Gingras, A.-C., Abe, K. T. & Raught, B. Getting to know the neighborhood: using proximity-dependent biotinylation to characterize protein complexes and map organelles. *Curr. Opin. Chem. Biol.* **48**, 44–54 (2019).
- Kim, D. I. & Roux, K. J. Filling the Void: Proximity-Based Labeling of Proteins in Living Cells. *Trends Cell Biol.* **26**, 804–817 (2016).
- Saini, P. & Courtneidge, S. A. Tks adaptor proteins at a glance. *J Cell Sci* **131**, jcs203661 (2018).
- Seals, D. F. *et al.* The adaptor protein Tks5/Fish is required for podosome formation and function, and for the protease-driven invasion of cancer cells. *Cancer Cell* **7**, 155–165 (2005).
- Cejudo-Martin, P. *et al.* Genetic disruption of the sh3pxd2a gene reveals an essential role in mouse development and the existence of a novel isoform of tks5. *PLoS One* **9**, e107674 (2014).
- Li, C. M.-C. *et al.* Differential Tks5 isoform expression contributes to metastatic invasion of lung adenocarcinoma. *Genes Dev.* **27**, 1557–1567 (2013).
- Lock, P., Abram, C. L., Gibson, T. & Courtneidge, S. A. A new method for isolating tyrosine kinase substrates used to identify fish, an SH3 and PX domain-containing protein, and Src substrate. *EMBO J.* **17**, 4346–4357 (1998).
- Blouw, B. *et al.* The invadopodia scaffold protein Tks5 is required for the growth of human breast cancer cells *in vitro* and *in vivo*. *PLoS One* **10**, e0121003 (2015).
- Burger, K. L. *et al.* Src-Dependent Tks5 Phosphorylation Regulates Invadopodia-Associated Invasion in Prostate Cancer Cells. *The Prostate* **74**, 134–148 (2014).
- Iizuka, S., Abdullah, C., Buschman, M. D., Diaz, B. & Courtneidge, S. A. The role of Tks adaptor proteins in invadopodia formation, growth and metastasis of melanoma. *Oncotarget* **7**, 78473–78486 (2016).
- Stylli, S. S., I, S. T. T., Kaye, A. H. & Lock, P. Prognostic significance of Tks5 expression in gliomas. *J. Clin. Neurosci.* **19**, 436–442 (2012).
- Oikawa, T., Itoh, T. & Takenawa, T. Sequential signals toward podosome formation in NIH-src cells. *J. Cell Biol.* **182**, 157–169 (2008).
- Abram, C. L. *et al.* The Adaptor Protein Fish Associates with Members of the ADAMs Family and Localizes to Podosomes of Src-transformed Cells. *J. Biol. Chem.* **278**, 16844–16851 (2003).
- Jacob, A., Linklater, E., Bayless, B. A., Lyons, T. & Prekeris, R. The role and regulation of Rab40b–Tks5 complex during invadopodia formation and cancer cell invasion. *J. Cell Sci.* **129**, 4341–4353 (2016).
- Diaz, B. *et al.* Tks5-Dependent, Nox-Mediated Generation of Reactive Oxygen Species Is Necessary for Invadopodia Formation. *Sci. Signal.* **2**, ra53–ra53 (2009).
- Stylli, S. S. *et al.* Nck adaptor proteins link Tks5 to invadopodia actin regulation and ECM degradation. *J. Cell Sci.* **122**, 2727–2740 (2009).
- Oser, M., Dovas, A., Cox, D. & Condeelis, J. Nck1 and Grb2 localization patterns can distinguish invadopodia from podosomes. *Eur. J. Cell Biol.* **90**, 181–188 (2011).
- Jeannot, P. & Besson, A. Cortactin function in invadopodia. *Small GTPases* 1–15. <https://doi.org/10.1080/21541248.2017.1405773> (2017).
- Ayala, I. *et al.* Faciogenital dysplasia protein Fgd1 regulates invadopodia biogenesis and extracellular matrix degradation and is up-regulated in prostate and breast cancer. *Cancer Res.* **69**, 747–752 (2009).
- Daubon, T., Buccione, R. & Génot, E. The Aarskog-Scott syndrome protein Fgd1 regulates podosome formation and extracellular matrix remodeling in transforming growth factor β -stimulated aortic endothelial cells. *Mol. Cell. Biol.* **31**, 4430–4441 (2011).
- Tsuboi, S. *et al.* FBP17 Mediates a Common Molecular Step in the Formation of Podosomes and Phagocytic Cups in Macrophages. *J. Biol. Chem.* **284**, 8548–8556 (2009).
- Yamamoto, H. *et al.* Requirement for FBP17 in invadopodia formation by invasive bladder tumor cells. *J. Urol.* **185**, 1930–1938 (2011).
- Suman, P., Mishra, S. & Chander, H. High expression of FBP17 in invasive breast cancer cells promotes invadopodia formation. *Med. Oncol. Northwood Lond. Engl.* **35**, 71 (2018).
- Carmona, G. *et al.* Lamellipodin promotes invasive 3D cancer cell migration via regulated interactions with Ena/VASP and SCAR/WAVE. *Oncogene* **35**, 5155–5169 (2016).

34. Boateng, L. R., Cortesio, C. L. & Huttenlocher, A. Src-mediated phosphorylation of mammalian Abp1 (DBNL) regulates podosome rosette formation in transformed fibroblasts. *J. Cell Sci.* **125**, 1329–1341 (2012).
35. Dekky, B., Ruff, M., Bonnier, D., Legagneux, V. & Th  ret, N. Proteomic screening identifies the zonula occludens protein ZO-1 as a new partner for ADAM12 in invadopodia-like structures. *Oncotarget* **9**, 21366–21382 (2018).
36. Kremerskothen, J. *et al.* Zona occludens proteins modulate podosome formation and function. *FASEB J.* **25**, 505–514 (2011).
37. Zhong, J. L. *et al.* Distinct functions of natural ADAM-15 cytoplasmic domain variants in human mammary carcinoma. *Mol. Cancer Res. MCR* **6**, 383–394 (2008).
38. Albrechtsen, R., Stautz, D., Sanjay, A., Kveiborg, M. & Wewer, U. M. Extracellular engagement of ADAM12 induces clusters of invadopodia with localized ectodomain shedding activity. *Exp. Cell Res.* **317**, 195–209 (2011).
39. Eckert, M. A. *et al.* ADAM12 induction by Twist1 promotes tumor invasion and metastasis via regulation of invadopodia and focal adhesions. *J. Cell Sci.* **130**, 2036–2048 (2017).
40. Kim, H.-Y., Ha Thi, H. T. & Hong, S. IMP2 and IMP3 cooperate to promote the metastasis of triple-negative breast cancer through destabilization of progesterone receptor. *Cancer Lett.* **415**, 30–39 (2018).
41. Vikesaa, J. *et al.* RNA-binding IMPs promote cell adhesion and invadopodia formation. *EMBO J.* **25**, 1456–1468 (2006).
42. Ben-Chetrit, N. *et al.* Synaptojanin 2 is a druggable mediator of metastasis and the gene is overexpressed and amplified in breast cancer. *Sci. Signal.* **8**, ra7 (2015).
43. Chuang, Y.-Y. *et al.* Role of synaptojanin 2 in glioma cell migration and invasion. *Cancer Res.* **64**, 8271–8275 (2004).
44. Nam, J.-M. *et al.* CIN85, a Cbl-interacting protein, is a component of AMAP1-mediated breast cancer invasion machinery. *EMBO J.* **26**, 647–656 (2007).
45. Schanda, K. *et al.* Nogo-B is associated with cytoskeletal structures in human monocyte-derived macrophages. *BMC Res. Notes* **4**, 6 (2011).
46. Rodr  guez-Feo, J. A., Gallego-Delgado, J., Puerto, M., Wandosell, F. & Osende, J. Reticulon-4B/Nogo-B acts as a molecular linker between microtubules and actin cytoskeleton in vascular smooth muscle cells. *Biochim. Biophys. Acta* **1863**, 1985–1995 (2016).
47. Vallenius, T. *et al.* The PDZ-LIM protein RIL modulates actin stress fiber turnover and enhances the association of alpha-actinin with F-actin. *Exp. Cell Res.* **293**, 117–128 (2004).
48. Vanaja, D. K. *et al.* PDLIM4, an actin binding protein, suppresses prostate cancer cell growth. *Cancer Invest.* **27**, 264–272 (2009).
49. Rosslenbroich, V. *et al.* Collapsin response mediator protein-4 regulates F-actin bundling. *Exp. Cell Res.* **310**, 434–444 (2005).
50. Dang, I. *et al.* Inhibitory signalling to the Arp2/3 complex steers cell migration. *Nature* **503**, 281–284 (2013).
51. Wilson, A. L., Schrecengost, R. S., Guerrero, M. S., Thomas, K. S. & Bouton, A. H. Breast cancer antiestrogen resistance 3 (BCAR3) promotes cell motility by regulating actin cytoskeletal and adhesion remodeling in invasive breast cancer cells. *PLoS One* **8**, e65678 (2013).
52. Cai, D. *et al.* AND-34/BCAR3, a GDP exchange factor whose overexpression confers antiestrogen resistance, activates Rac, PAK1, and the cyclin D1 promoter. *Cancer Res.* **63**, 6802–6808 (2003).
53. Bauer, K. *et al.* Human CLP36, a PDZ-domain and LIM-domain protein, binds to alpha-actinin-1 and associates with actin filaments and stress fibers in activated platelets and endothelial cells. *Blood* **96**, 4236–4245 (2000).
54. Liu, Z. *et al.* PDZ and LIM domain protein 1 (PDLIM1)/CLP36 promotes breast cancer cell migration, invasion and metastasis through interaction with alpha-actinin. *Oncogene* **34**, 1300–1311 (2015).
55. Masi, G. *et al.* p66Shc regulates vesicle-mediated secretion in mast cells by affecting F-actin dynamics. *J. Leukoc. Biol.* **95**, 285–292 (2014).
56. Lin, Y.-H. *et al.* LIMCH1 regulates nonmuscle myosin-II activity and suppresses cell migration. *Mol. Biol. Cell* **28**, 1054–1065 (2017).
57. Mizoguchi, T., Ikeda, S., Watanabe, S., Sugawara, M. & Itoh, M. Mib1 contributes to persistent directional cell migration by regulating the Ctnd1-Rac1 pathway. *Proc. Natl. Acad. Sci. USA* **114**, E9280–E9289 (2017).
58. Matsushima, K., Tokuraku, K., Hasan, M. R. & Kotani, S. Microtubule-associated protein 4 binds to actin filaments and modulates their properties. *J. Biochem. (Tokyo)* **151**, 99–108 (2012).
59. Werner, E., Kowalczyk, A. P. & Faundez, V. Anthrax toxin receptor 1/tumor endothelium marker 8 mediates cell spreading by coupling extracellular ligands to the actin cytoskeleton. *J. Biol. Chem.* **281**, 23227–23236 (2006).
60. Garlick, K. M. & Mogridge, J. Direct interaction between anthrax toxin receptor 1 and the actin cytoskeleton. *Biochemistry* **48**, 10577–10581 (2009).
61. Sharma, V. P. *et al.* Tks5 and SHIP2 regulate invadopodium maturation, but not initiation, in breast carcinoma cells. *Curr. Biol. CB* **23**, 2079–2089 (2013).
62. Oikawa, T. *et al.* Tks5-dependent formation of circumferential podosomes/invadopodia mediates cell–cell fusion. *J. Cell Biol.* **197**, 553–568 (2012).
63. Kuo, J.-C., Han, X., Hsiao, C.-T., Yates, J. R. & Waterman, C. M. Analysis of the myosin-II-responsive focal adhesion proteome reveals a role for beta-Pix in negative regulation of focal adhesion maturation. *Nat. Cell Biol.* **13**, 383–393 (2011).
64. Kim, D. I. *et al.* Probing nuclear pore complex architecture with proximity-dependent biotinylation. *Proc. Natl. Acad. Sci. USA* **111**, E2453–E2461 (2014).
65. Attanasio, F. *et al.* Novel invadopodia components revealed by differential proteomic analysis. *Eur. J. Cell Biol.* **90**, 115–127 (2011).
66. Cervero, P., Himmel, M., Kr  ger, M. & Linder, S. Proteomic analysis of podosome fractions from macrophages reveals similarities to spreading initiation centres. *Eur. J. Cell Biol.* **91**, 908–922 (2012).
67. Ezzoukhry, Z. *et al.* Combining laser capture microdissection and proteomics reveals an active translation machinery controlling invadosome formation. *Nat. Commun.* **9**, 2031 (2018).
68. Branon, T. C. *et al.* Efficient proximity labeling in living cells and organisms with TurboID. *Nat. Biotechnol.* **36**, 880–887 (2018).
69. Kim, D. I. *et al.* An improved smaller biotin ligase for BioID proximity labeling. *Mol. Biol. Cell* **27**, 1188–1196 (2016).
70. Di Martino, J. *et al.* The microenvironment controls invadosome plasticity. *J. Cell Sci.* **129**, 1759–1768 (2016).
71. Juin, A. *et al.* Physiological type I collagen organization induces the formation of a novel class of linear invadosomes. *Mol. Biol. Cell* **23**, 297–309 (2012).
72. Lam, S. S. *et al.* Directed evolution of APEX2 for electron microscopy and proximity labeling. *Nat. Methods* **12**, 51–54 (2015).
73. Brudvig, J. J. *et al.* MARCKS Is Necessary for Netrin-DCC Signaling and Corpus Callosum Formation. *Mol. Neurobiol.* **55**, 8388–8402 (2018).
74. Dingar, D. *et al.* BioID identifies novel c-MYC interacting partners in cultured cells and xenograft tumors. *J. Proteomics* **118**, 95–111 (2015).
75. Uezu, A. *et al.* Identification of an elaborate complex mediating postsynaptic inhibition. *Science* **353**, 1123–1129 (2016).
76. Shevchenko, A., Wilm, M., Vorm, O. & Mann, M. Mass spectrometric sequencing of proteins silver-stained polyacrylamide gels. *Anal. Chem.* **68**, 850–858 (1996).
77. Cox, J. & Mann, M. MaxQuant enables high peptide identification rates, individualized p.p.b.-range mass accuracies and proteome-wide protein quantification. *Nat. Biotechnol.* **26**, 1367–1372 (2008).
78. Cox, J. *et al.* Accurate proteome-wide label-free quantification by delayed normalization and maximal peptide ratio extraction, termed MaxLFQ. *Mol. Cell. Proteomics MCP* **13**, 2513–2526 (2014).
79. Cox, J. *et al.* Andromeda: a peptide search engine integrated into the MaxQuant environment. *J. Proteome Res.* **10**, 1794–1805 (2011).

80. Tusher, V. G., Tibshirani, R. & Chu, G. Significance analysis of microarrays applied to the ionizing radiation response. *Proc. Natl. Acad. Sci. USA* **98**, 5116–5121 (2001).
81. Deutsch, E. W. *et al.* The ProteomeXchange consortium in 2017: supporting the cultural change in proteomics public data deposition. *Nucleic Acids Res.* **45**, D1100–D1106 (2017).
82. Vizcaino, J. A. *et al.* ProteomeXchange provides globally coordinated proteomics data submission and dissemination. *Nat. Biotechnol.* **32**, 223–226 (2014).
83. Mi, H., Muruganujan, A., Ebert, D., Huang, X. & Thomas, P. D. PANTHER version 14: more genomes, a new PANTHER GO-slim and improvements in enrichment analysis tools. *Nucleic Acids Res.* **47**, D419–D426 (2019).
84. Mi, H. *et al.* Protocol Update for large-scale genome and gene function analysis with the PANTHER classification system (v.14.0). *Nat. Protoc.* **14**, 703–721 (2019).
85. Supek, F., Bošnjak, M., Škunca, N. & Šmuc, T. REVIGO summarizes and visualizes long lists of gene ontology terms. *PLoS One* **6**, e21800 (2011).
86. von Mering, C. *et al.* STRING: known and predicted protein-protein associations, integrated and transferred across organisms. *Nucleic Acids Res.* **33**, D433–437 (2005).
87. Szklarczyk, D. *et al.* STRING v11: protein-protein association networks with increased coverage, supporting functional discovery in genome-wide experimental datasets. *Nucleic Acids Res.* **47**, D607–D613 (2019).

Acknowledgements

We thank D. Isnardon and M. Rodriguez (CRCM Microscopy Platform) for support and S.A. Courtneidge, K.J. Roux and C. Lachaud for sharing reagents. This work was supported by Canceropôle Provence-Alpes-Côte d'Azur (PACA), Institut National du Cancer, Conseil Régional PACA and Site de Recherche Intégrée sur le Cancer (SIRIC). Proteomic analyses were performed at the mass spectrometry facility of Marseille Proteomics supported by IBISA (Infrastructures Biologie Santé et Agronomie), Plateforme Technologique Aix-Marseille, Canceropôle PACA, Région Sud Provence-Alpes-Côte d'Azur, Fonds Européen de Développement Régional (FEDER) and Plan Cancer.

Author contributions

S.T. and A.B. designed research; S.T., C.M., J.S., K.O., B.C., D.S. and E.B. performed research; S.T., C.M., J.S., K.O., B.C., S.A., L.C. and A.B. analyzed data; S.T. and A.B. wrote the paper.

Competing interests

The authors declare no competing interests.

Additional information

Supplementary information is available for this paper at <https://doi.org/10.1038/s41598-020-63926-4>.

Correspondence and requests for materials should be addressed to S.T.

Reprints and permissions information is available at www.nature.com/reprints.

Publisher's note Springer Nature remains neutral with regard to jurisdictional claims in published maps and institutional affiliations.



Open Access This article is licensed under a Creative Commons Attribution 4.0 International License, which permits use, sharing, adaptation, distribution and reproduction in any medium or format, as long as you give appropriate credit to the original author(s) and the source, provide a link to the Creative Commons license, and indicate if changes were made. The images or other third party material in this article are included in the article's Creative Commons license, unless indicated otherwise in a credit line to the material. If material is not included in the article's Creative Commons license and your intended use is not permitted by statutory regulation or exceeds the permitted use, you will need to obtain permission directly from the copyright holder. To view a copy of this license, visit <http://creativecommons.org/licenses/by/4.0/>.

© The Author(s) 2020